



Electrochemistry Hot Paper

How to cite:

International Edition: doi.org/10.1002/anie.202110000

German Edition: doi.org/10.1002/ange.202110000

In Situ Phase Separation into Coupled Interfaces for Promoting CO₂ Electroreduction to Formate over a Wide Potential Window

Wenbin Wang, Zhitong Wang, Ruouo Yang, Junyuan Duan, Youwen Liu,* Anmin Nie, Huiqiao Li, Bao Yu Xia, and Tianyou Zhai*

Abstract: Bimetallic sulfides are expected to realize efficient CO₂ electroreduction into formate over a wide potential window, however, they will undergo in situ structural evolution under the reaction conditions. Therefore, clarifying the structural evolution process, the real active site and the catalytic mechanism is significant. Here, taking Cu₂SnS₃ as an example, we unveiled that Cu₂SnS₃ occurred self-adapted phase separation toward forming the stable SnO₂@CuS and SnO₂@Cu₂O heterojunction during the electrochemical process. Calculations illustrated that the strongly coupled interfaces as real active sites driven the electron self-flow from Sn⁴⁺ to Cu⁺, thereby promoting the delocalized Sn sites to combine HCOO* with H*. Cu₂SnS₃ nanosheets achieve over 83.4% formate selectivity in a wide potential range from -0.6 V to -1.1 V. Our findings provide insight into the structural evolution process and performance-enhanced origin of ternary sulfides under the CO₂ electroreduction.

Introduction

Electrochemical CO₂ reduction reaction (CO₂RR) is an emerging and promising pathway to tackle the challenges of environmental degradation and the depletion of fossil fuels, which can utilize the renewable electricity originating from the intermittent renewable energy (such as solar, wind, and tidal energy) to drive CO₂ into value-added chemical products.^[1] Among the products, the C₁ (CO and formate)

products, especially formate is an important chemicals, which has a potential industrial application in direct fuel cells, hydrogen storage and the synthesis of chemical products.^[2] Developing a practical electrocatalysts for driving CO₂ to formate needs to overcome the conundrum of the large reorganizational energy of CO₂ and the involved multiple reaction pathway of CO₂RR.^[3] Among the reported catalysts for CO₂RR, Sn-based catalysts present well-matched affinity to the key intermediate HCOO*.^[4] Accordingly, Sn-based catalysts were exploited to obtain formate. However, in theory, the active Sn⁴⁺ sites of Sn-based catalysts tend to be reduced irreversibly under the negative potential.^[5] As a consequence, some of them realize a high selectivity for formate only on extremely narrow potential window and suffer from poor stability.^[6]

Considering the difference of the redox potential between Cu⁺ and Sn⁴⁺, the Cu⁺ is easier reduced than Sn⁴⁺ toward protecting the highly active Sn⁴⁺ from reduction under the applied negative potential.^[7] Therefore, there is a viable way to resolve the unstable property of Sn⁴⁺ by constructing Cu-Sn catalysts which possess strong electron interaction between Cu⁺ and Sn⁴⁺. Meanwhile, the introduction of Cu is also expected to regulate the electron state of Sn, further optimizing the ability to capture absorbates.^[8] In this regard, bimetallic sulfides (such as Cu₂SnS₃) maybe a reliable platform for realizing efficient CO₂ electroreduction into formate over a wide potential window, which could maximize the modulation effect of Cu⁺ on Sn⁴⁺ due to their tunable composition and uniform composition distribution.^[9]

Notably, it has been proved both experimentally and theoretically that metal sulfides are very sensitive and may undergo structural evolution to form biphasic sulfide- or oxide- and -metal catalysts during the electrochemical process.^[10] Consequently, some new highly active phases and highly active local structures,^[7c,11] such as, heterogeneous interface,^[12] inter-particle grain boundaries and vacancies^[13] will be created along with this in situ structural evolution, which will be as actual active sites to trigger efficient catalytic reaction. However, due to the complex chemical environment and high potential dependence of this structural evolution process,^[5a] it is difficult to clearly reveal the structural evolution process, the real active site and the catalytic mechanism of metal sulfides during the CO₂RR process, thereby limiting the design and development of the catalysts with high activity and stability. Therefore, it would be a huge opportunity to obtain an excellent Cu-Sn based catalysts from bimetallic sulfides through in situ self-optimized strategy, thereby realizing efficient conversion of CO₂ to formate over

[*] W. B. Wang, R. O. Yang, Dr. J. Y. Duan, Dr. Y. W. Liu, Prof. H. Q. Li, Prof. T. Y. Zhai

State Key Laboratory of Materials Processing and Die & Mould Technology, and School of Materials Science and Engineering, Huazhong University of Science and Technology
Wuhan, Hubei, 430074 (P. R. China)
E-mail: zhaity@hust.edu.cn
ywliu@hust.edu.cn

Z. T. Wang, Prof. B. Y. Xia
Key Laboratory of Material Chemistry for Energy Conversion and Storage (Ministry of Education), Hubei Key Laboratory of Material Chemistry and Service Failure, Wuhan National Laboratory for Optoelectronics, School of Chemistry and Chemical Engineering, Huazhong University of Science and Technology
Wuhan, Hubei, 430074 (P. R. China)

Prof. A. M. Nie
Center for High Pressure Science, State Key Laboratory of Metastable Materials Science and Technology, Yanshan University
Qinhuangdao, Hebei, 066004 (P. R. China)

Supporting information and the ORCID identification number(s) for the author(s) of this article can be found under:
<https://doi.org/10.1002/anie.202110000>.

a wide potential window, but uncovering the real relationship between the structure and activity is still a great challenge.

Herein, we synthesized ultrathin Cu_2SnS_3 nanosheets as catalysts and realized a high selectivity and activity for CO_2RR to formate in the wide potential range from -0.6 V to -1.1 V. The high-angle annular dark-field scanning TEM (HAADF-STEM) images and X-ray absorption near-edge structure (XANES) uncovered that Cu_2SnS_3 nanosheets can transfer to the CuS@SnO_2 and $\text{Cu}_2\text{O@SnO}_2$ through in situ electroreduction driven self-adapted transformation. On the basis of clarifying the real catalytic sites, density-functional theory (DFT) calculations revealed that the electron of Sn^{4+} tend to delocalize and donate to Cu^+ via the O atom by the formation of heterojunction interface between in SnO_2 and $\text{CuS/Cu}_2\text{O}$. The delocalized Sn sites not only can enhance the affinity for the HCOO^* and promote the dissociation of H_2O to form H^* , but also stabilize the active Sn^{4+} sites for resisting the applied negative potential, thereby improving the activity and selectivity for CO_2RR in a wide potential window. Explicit real active site and clear structure–activity relationship in this work will provide an inspiration for designing an ideal electrocatalysts suitable for a wide operated potential window.

Results and Discussion

We started with the preparation of ultrathin Cu_2SnS_3 nanosheets with monoclinic structure. As shown in Figure 1 a, the monoclinic structure consists of pseudo-tetrahedron where all sites are distorted and cations are coordinated by S atom. A facile hydrothermal reaction was used here to fabricate ultrathin Cu_2SnS_3 nanosheets in the absence of surfactant. Figure 1 b shows the transmission electron microscopy (TEM) image of as prepared products, which present an ultrathin nanosheets with a horizontal size of approximately 50 nm. High-resolution TEM (HRTEM) images (Figure 1 c) revealed distinct lattice fringes with an interplanar spaces of 0.309 nm, corresponding to the (002) plane of monoclinic Cu_2SnS_3 phase.^[9] In addition, the X-ray diffraction (XRD) pattern of as prepared products matched the characteristic peaks of monoclinic Cu_2SnS_3 materials (Figure S1).^[14] Fur-

thermore, the average thickness of the obtained materials were determined to be around 4.4 nm (Figure 1 d). The Cu, Sn and S elements were homogeneous spatial distributions throughout the ultrathin nanosheets (Figure 1 e and f), while the O element may be due to the partial oxidation of the ultrathin Cu_2SnS_3 nanosheets by the air.^[15] Thus, these results indicate the successful fabrication of ultrathin Cu_2SnS_3 nanosheets with monoclinic structure.

The CO_2RR performance of the obtained ultrathin Cu_2SnS_3 nanosheets was explored in a flow cell with 0.5 M KHCO_3 electrolyte (Figure 2 a–e). To investigate the role of Cu and Sn in Cu_2SnS_3 during the CO_2RR process, CuS and SnS_2 as the contrast sample were also explored (Figure S2 a–c, S3 a–c and S4). Interestingly, the difference of linear sweep voltammetry (LSV) curves between the initial state and stable state in all catalysts (Cu_2SnS_3 , CuS and SnS_2) suggested that all catalysts were suffer from the in situ phase transformation during the CO_2RR process (Figure S5). After obtained the stable LSV curves, the CO_2RR performance was evaluated. Obviously, the CO_2RR activity of ultrathin Cu_2SnS_3 nanosheets is more favorable than that of HER (Figure S6). Particularly, ultrathin Cu_2SnS_3 nanosheets presented higher selectivity for CO_2RR to formate than CuS and SnS_2 (Figure 2 a). Apparently, the Faradic efficiency (FE) of formate is keep more than 80% for ultrathin Cu_2SnS_3 nanosheets in a wide potential window from -0.65 to -1.1 V vs. RHE. Meanwhile, its total FE of C_1 products (formate and CO) is approach about 90% in the same wide potential range (Figure 2 d). Different from CuS and SnS_2 , the main product of Cu_2SnS_3 electroreduction CO_2 is formate (Figures 2 b, S7). Undoubtedly, the relative change of the partial current density for formate, CO and H_2 indicate that the local electrochemical environment of Cu atom and Sn atom in Cu_2SnS_3 is different from that of CuS and SnS_2 (Figure 2 c and S8, S9). It cannot be ignored that the total FE of CuS and SnS_2 for CO_2RR is far less than 100%, which exceeds the measurement error range. This abnormal phenomenon may be attributed to the fact that the cation was reduced under the reduction potential and consumed part of the charge originally applied to CO_2RR process.^[5a,c,16] Furthermore, the reduction effect of this cation in CuS and SnS_2 is also persistent (Figure S10), which may be attributed to the balance between the activation of the active O and the reduction effect of the cation. Nevertheless, the total FE of Cu_2SnS_3 close to 100% indicate that the synergistic effect of Cu and Sn atoms promotes higher affinity between cations in Cu_2SnS_3 and CO_2 molecules and enhances its catalytic efficiency. As shown in Figure 2 e, both the current density and the FEs of CO and H_2 are apparently unchanged in a 10 h potentiostat test. Meanwhile, the selectivity for formate and C_1 are 84.1% and 92.5%, respectively. The high FEs, large current density, stable selectivity and durable activity for CO_2RR all suggested that Cu_2SnS_3 has a more favorable and stable activated state than CuS and SnS_2 . To further evaluate the tolerance of activated state of Cu_2SnS_3 for CO_2RR in the wide potential window under alkaline condition, 1 M KOH solutions was adopted to investigate the variation of selectivity and FEs for CO, H_2 , and formate on Cu_2SnS_3 catalysts. Remarkably, the FE for formate and C_1 have been growing

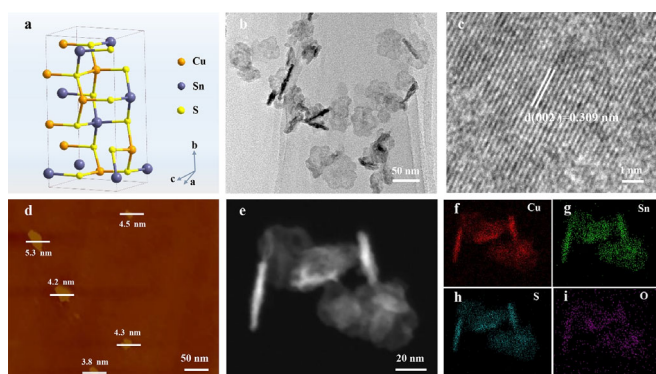


Figure 1. Structural analysis of Cu_2SnS_3 . a) Crystal structure, b), c) TEM and HRTEM images, d) AFM image, e) HAADF-STEM image, and f)–i) corresponding EDX element mapping.



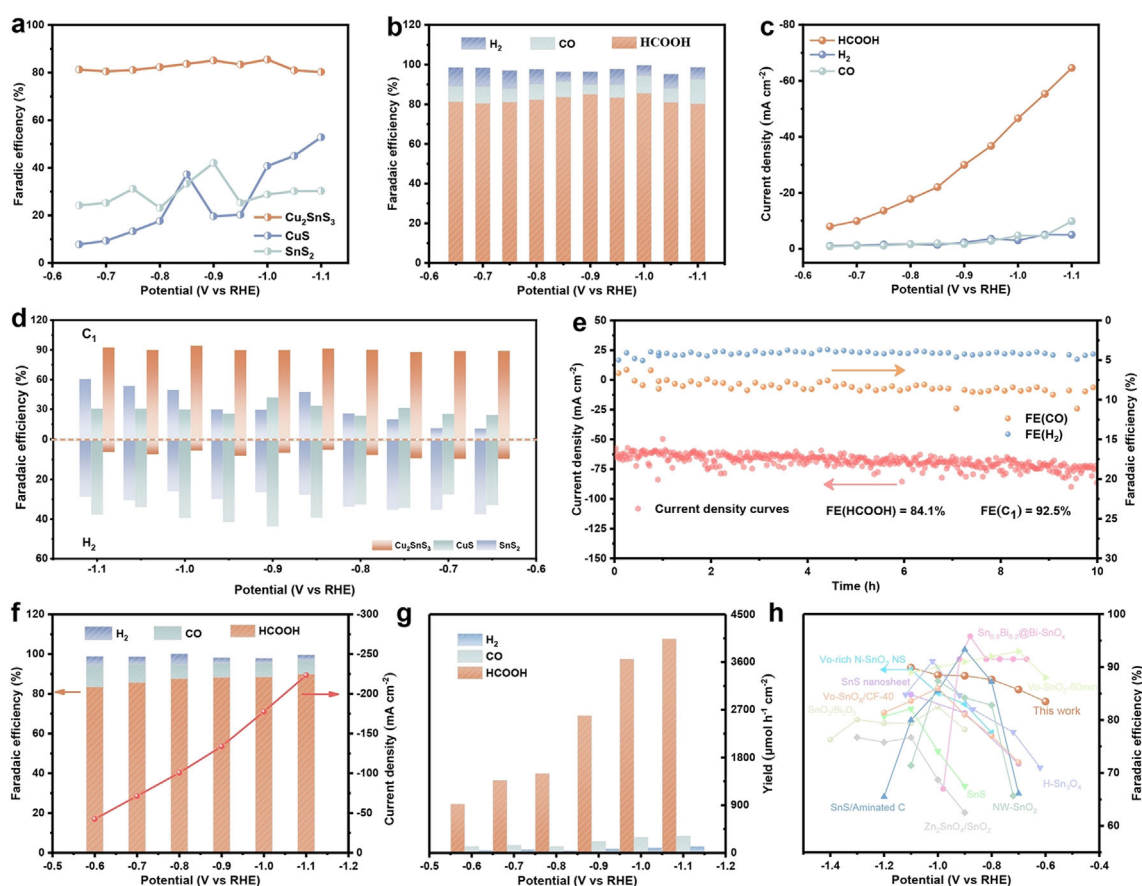


Figure 2. CO₂RR performance a) FE of HCOOH. b) FE of HCOOH, CO and H₂ for the Cu₂SnS₃. c) Partial current density of HCOOH, CO and H₂ on the Cu₂SnS₃. d) FE of C₁ and H₂. e) A 10 h potentiostat test for the Cu₂SnS₃ at 1.0 V. f) The CO₂RR performance and g) The formation rates of HCOOH, CO and H₂ on the Cu₂SnS₃ in 1 M KOH electrolyte. h) FE of HCOOH comparison among the reported oxidation state Sn-based catalysts and the Cu₂SnS₃. The FE dates come from (f).

with the potential raising and the values reaching above 83.4% and 95.5% in the potential range from -0.6 V to -1.1 V (Figure 2f and S12), respectively. Moreover, the selectivity of CO₂RR to formate reached the highest FE of 89.9% with the largest yield rate of $4038.9 \mu\text{mol h}^{-1} \text{cm}^{-2}$ at -1.1 V (Figure 2g). By contrast, the yield rate for CO and H₂ has been negligible, suggesting that Cu₂SnS₃ possess excellent selectivity and activity for CO₂RR to formate. Compared with the reported oxidation state Sn-based catalysts, Cu₂SnS₃ catalysts exhibit a promising combination of high activity and selectivity for CO₂ to formate over the wide potential windows from -0.6 V to -1.1 V (Figure 2h).^[5b,6b,10a,17] What's more, its current density with and without IR compensation is excellent compared to the reported catalysts in flow cell (Figure S11 and Table S1).

The exhibited performance of catalysts depends on its self-adjusting state during the electrocatalytic process. Thus, to unravel the superiority of the adaptive state of Cu₂SnS₃ for CO₂RR, the chemical state and structure of the catalysts was investigated after CO₂RR. As shown in Figure 3a, the nanosheet-like morphology of Cu₂SnS₃ was reserved after CO₂RR (the Cu₂SnS₃ after CO₂RR denoted as R-Cu₂SnS₃). Unlike the smooth surface of the pristine Cu₂SnS₃ (P-Cu₂SnS₃), HAADF-STEM images shows that the dense

nanoparticles are anchored on the surface of the nanosheets for R-Cu₂SnS₃ (Figure 3b). Observing, the core area of the nanosheets exhibit a lattice fringe distance of 0.304 nm, according with the (102) plane of hexagonal CuS (Figure 3d and e). However, the lattice spacing of 0.243 nm and 0.328 nm was observed in the edge of the nanosheets (Figure 3b, c and f), which consistent with the (111) plane of Cu₂O and the (110) plane of SnO₂, respectively. Meanwhile, there are many amorphous phases wrapping in the surface of nanosheets (Figure 3c–f). All these results agreed with the XRD pattern of R-Cu₂SnS₃ (Figure S13). Interestingly, the distribution area of Cu and S is limited to the core of R-Cu₂SnS₃ nanosheets, but Sn and O adhere to the external surface of Cu and S (Figure 3g), which corresponding the regions where nanoparticles exist. Based on the above analysis, P-Cu₂SnS₃ nanosheets were transformed into CuS@SnO₂ heterojunction nanosheets with part of Cu₂O through in situ electroreduction driven self-adapt transformation. In view of the special sites and valence of Cu₂SnS₃, the formation principle of the heterojunction nanosheets is simply deduced (Figure 4a). During the CO₂RR process, Cu₂SnS₃ nanosheets undergo phase separation instantly when the reduction potential applied. In this process, the Sn⁴⁺ is easily drawn by the negative potential to migrate from the inside of the nanosheet

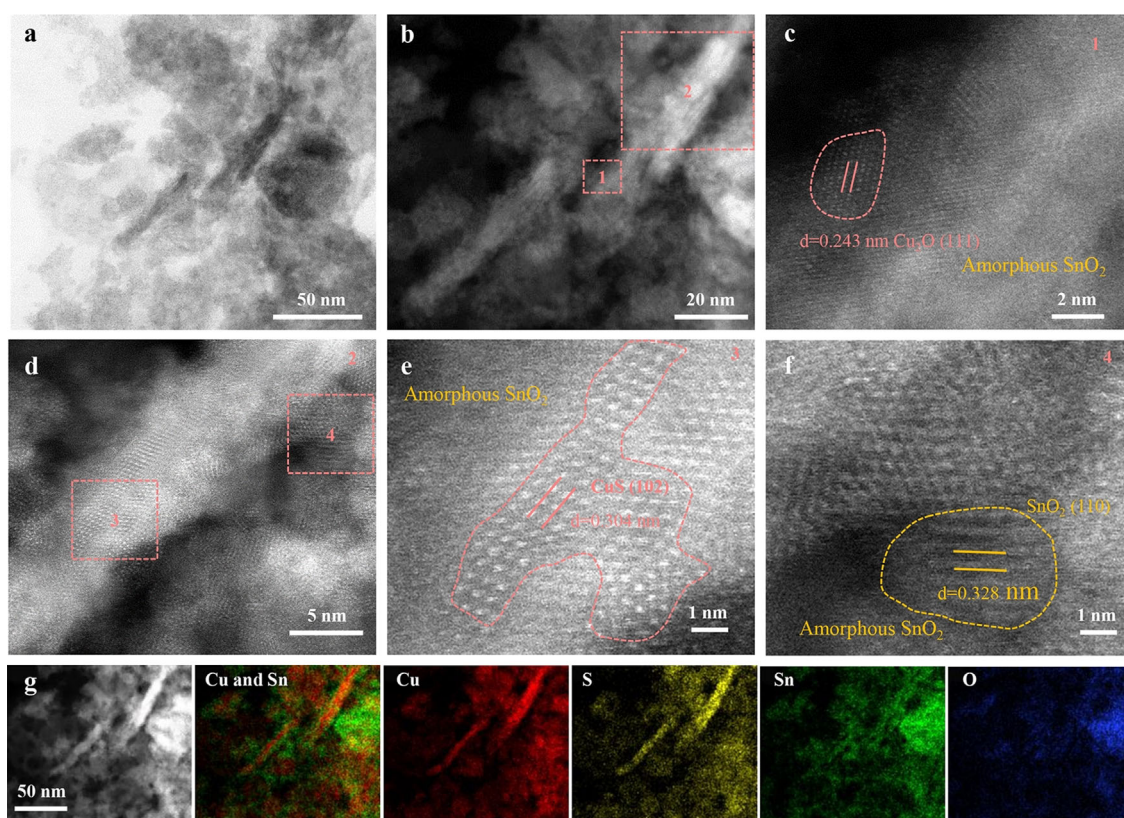


Figure 3. The characterization of the Cu_2SnS_3 after CO_2RR (R- Cu_2SnS_3). a) TEM image, b)–f) HAAD-STEM images, g) HAAD-STEM image and corresponding EDX element mapping for the R- Cu_2SnS_3 .

to the surface, and the coordinated S atoms are quickly replaced by the strong electronegative O to form SnO_2 nanoparticles. While Cu^+ carries the coordinated S atoms and shrinks to the central area and inherits the morphology of nanosheets to form CuS. Meanwhile, the dense SnO_2 nanoparticles anchored the surface of CuS nanosheets to form the heterojunction nanosheets by self-assembly, and prevent the complete oxidation of CuS. This adaptive formation of SnO_2 on heterojunction by this in situ electrochemical transformation from Cu_2SnS_3 also means that the highly active Sn^{4+} sites on heterojunction were still maintained under the applied potential and thus contribute to the high formate selectivity in the wide potential window.

To verify the formation rationality of the heterojunction nanosheets, Cu and Sn K-edge XANES were employed (Figure 4b–e). Obviously, the local coordination environments of the both Cu and Sn atom in R- Cu_2SnS_3 is different from that of P- Cu_2SnS_3 . The geometric local structure of Cu atoms seems to be the combination of the CuS and Cu_2O (Figure 4b), while the Sn in R- Cu_2SnS_3 tend to form the SnO_2 (Figure 4d). It is worth noting that the Cu–O peak and Cu–S peak was existed in R- Cu_2SnS_3 (Figure 4c), and the Sn–O peak and Sn–S peak also coexist (Figure 4e). Thus, these results suggested that the SnO_2 , CuS and Cu_2O were co-existed in R- Cu_2SnS_3 nanosheets. It was consistent with the conclusion obtained from the HAADF-STEM characterization, which is that R- Cu_2SnS_3 consist of CuS@SnO_2 and $\text{Cu}_2\text{O@SnO}_2$. What's more, the co-existed M–O peak and M–S

peak confirms that the heterojunction has strongly coupled interfaces effect, which further ensure the stability of the heterojunction after Cu_2SnS_3 suffer from phase transformation during the CO_2RR process. To further evaluate the role of chemical states in R- Cu_2SnS_3 , X-ray photoelectron spectroscopy (XPS) was performed. The negatively shift XPS peaks of Cu 2p and the constant XPS peaks of Sn 3d suggested that the formation of the heterojunction nanosheets can efficiently enhanced the negative potential tolerance of Sn^{4+} through the electron self-flow between Cu^+ and Sn^{4+} during the CO_2RR process (Figure 4f and g).^[8] These results also demonstrated that the Sn^{4+} held the same valence state during the CO_2RR process for it benefited from the protection of Cu^+ with more positive redox potential than Sn^{4+} and the strong electron interaction between the CuS, Cu_2O and SnO_2 (Figure S14).^[18] In theory, it is easier to reduction the Cu cations than Sn cations.^[19] Experimentally, the CuS was tend to form the $\text{Cu}_2\text{O@CuO}$ during the CO_2RR process, while the SnS_2 has evolved into the composites of Sn, SnO and Sn_2O_3 easily (Figure S2,S3 and S15,S17). Combined with the imperfect total FEs of CuS and SnS_2 , the cations reduction behavior in CuS and SnS_2 is a reversible reaction. This results in the portion charge which originally applied to CO_2 transfer process is consumed by the redox cycle of cations (Figure S7). In contrast, benefited from the electron interaction and the difference of redox potential between Cu^+ and Sn^{4+} in heterojunction, the Sn^{4+} of the SnO_2 on the surface of heterojunction has strong resistance to negative potential

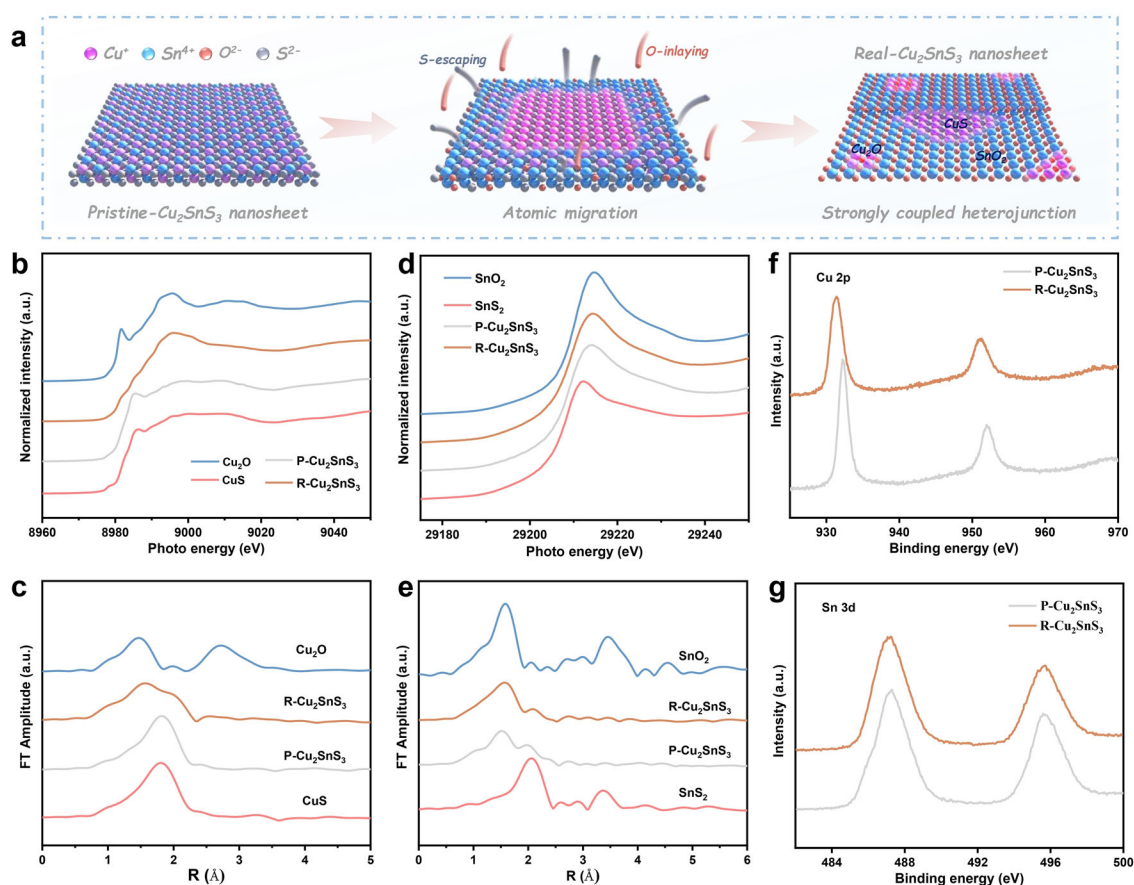


Figure 4. The characterization of the Cu_2SnS_3 before (P- Cu_2SnS_3) and after CO_2RR (R- Cu_2SnS_3). a) Diagram of the in situ transformation process. b) Cu K-edge XANES spectra and the corresponding FT curves (c). d) Sn K-edge XANES spectra and the corresponding FT curves (e) for Cu_2SnS_3 catalysts before and after CO_2RR . f) XPS Cu 2p spectra and g) Sn 3d spectra for Cu_2SnS_3 catalysts before and after CO_2RR .

during the CO_2RR process. Therefore, the R- Cu_2SnS_3 exhibited the stable activity and high selectivity for CO_2RR .

The stable heterojunction structure and mutually supporting chemical state provide perdurable and selective conversion of CO_2 . To elucidate the promote effect of heterojunction interface, DFT calculations were conducted to explore the thermochemical energetics of CO_2RR and HER on the surface of SnO_2 and the surface SnO_2 layer of CuS@SnO_2 and $\text{Cu}_2\text{O@SnO}_2$ (Figure S18–S20). The Gibbs free energies of reaction route for producing HCOOH, CO and H_2 are presented in Figure 5a–d. Obviously, the rate-determining step (RDS) for the HCOOH route is the process of HCOO^* to HCOOH in all model. The Gibbs free energies of the RDS for CuS@SnO_2 (0.58 eV) and $\text{Cu}_2\text{O@SnO}_2$ (0.25 eV) are much smaller than that of SnO_2 (2.24 eV), suggesting that the heterojunction are more likely to promote the formation of formate than SnO_2 . However, the RDS for CO route on SnO_2 is the CO^* desorption, while the RDS for CO route on heterojunction of CuS@SnO_2 and $\text{Cu}_2\text{O@SnO}_2$ are changed to the process from CO_2 (g) to COOH^* . The changed RDS pathway for the formation CO led to a raise in the energy barrier of the RDS on the surface of CuS@SnO_2 (1.34 eV) and $\text{Cu}_2\text{O@SnO}_2$ (1.58 eV), which is higher than that of SnO_2 (1.21 eV). The huge energy difference of the RDS pathway between HCOOH and CO on heterojunction indicate the

HCOOH route is more thermodynamics-favorable than the CO route, and hence clarify why the Cu_2SnS_3 exhibit high selectivity for HCOOH rather than that of CO in CO_2RR .^[20] Furthermore, the Gibbs free energies of H_2 is 1.47, 0.91 and 1.07 eV on the surface of SnO_2 , CuS@SnO_2 and $\text{Cu}_2\text{O@SnO}_2$ (Figure 5d), showing the weakened bonding strength between H^* and the surface of heterojunction.^[21] Meanwhile, the lower formation energy barrier of H_2 on CuS@SnO_2 and $\text{Cu}_2\text{O@SnO}_2$ suggest that the heterojunction can facilitate the dissociation of H_2O .^[22] Clearly, the Gibbs free energies of the RDS pathway for the formation HCOOH is much lower than that of H_2 on the surface of heterojunction. Thus, it can be inferred that the SnO_2 on the edge of the heterojunction nanosheets (CuS@SnO_2 and $\text{Cu}_2\text{O@SnO}_2$) can facilitate the process of CO_2 to HCOOH more efficiently. To further reveal the reason for the lowered energy barrier of the RDS on the heterojunction, the projected density of states (PDOS) was performed to explore the electron interaction between O atom in absorbed HCOO^* and the surface Sn atoms on catalyst models. As shown in Figure 5e, the heterojunction of CuS@SnO_2 and $\text{Cu}_2\text{O@SnO}_2$ present more harmonic p-p and p-d overlaps between the O p and Sn d, p orbitals below the Fermi level than SnO_2 , illustrating that Sn atoms on heterojunction of CuS@SnO_2 and $\text{Cu}_2\text{O@SnO}_2$ has a strong interaction with the O atom in absorbed HCOO^* .^[23] In addition,

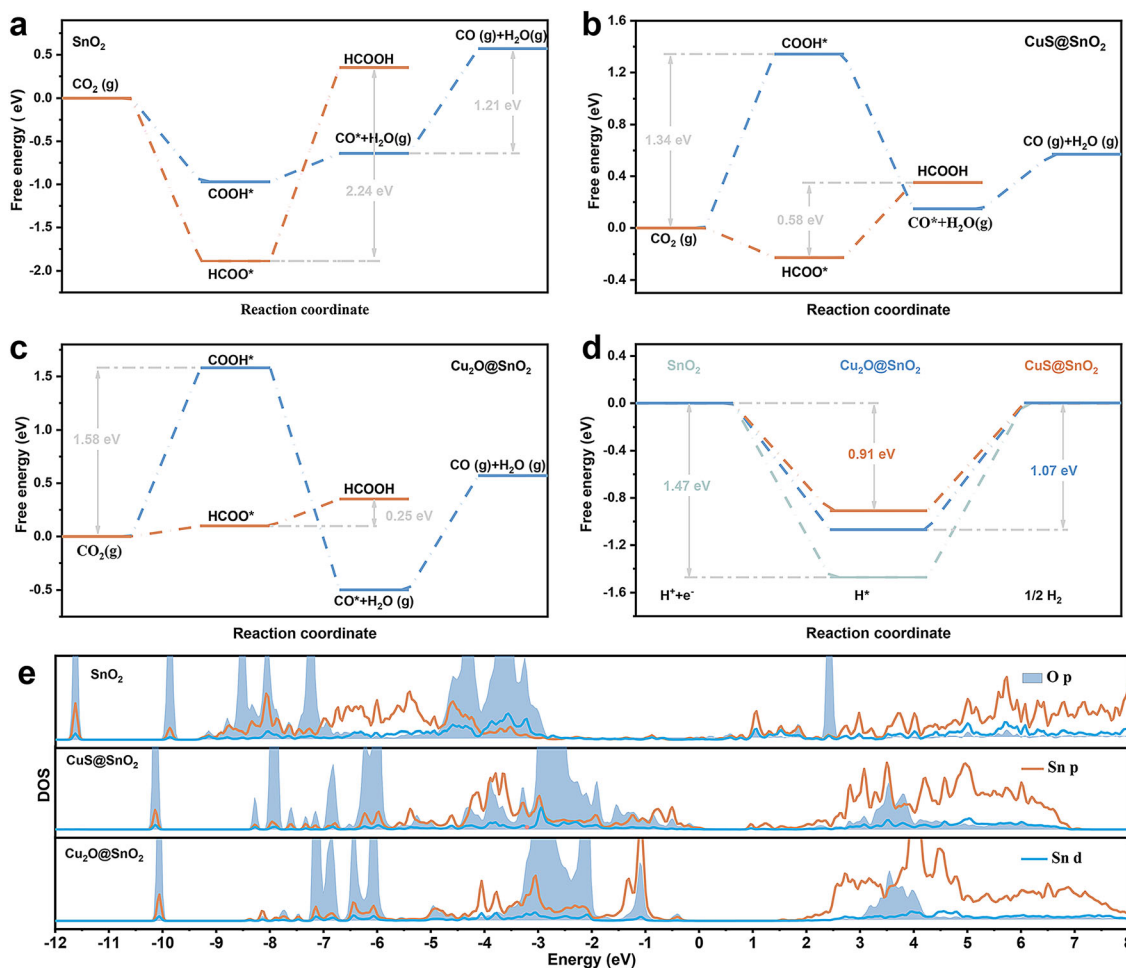


Figure 5. DFT calculation results. a)–c) Gibbs free energy diagrams for CO and HCOOH on SnO₂, CuS@SnO₂, and Cu₂O@SnO₂, respectively. d) Gibbs free energy diagrams for H₂ on SnO₂, CuS@SnO₂ and Cu₂O@SnO₂. e) Projected density of states (PDOS) of p and d orbitals of Sn atom and p orbitals of O atom on SnO₂, CuS@SnO₂ and Cu₂O@SnO₂ surfaces with adsorbed HCOO*.

the electron states of both the O p and Sn p, d orbitals are upshift away from the Fermi level after the formation of the heterojunction of CuS@SnO₂ and Cu₂O@SnO₂, which also indicates a strongest binding force between HCOO* and the heterojunction surface.^[24] Moreover, the upshift electron states of O p orbitals means that the O atom of HCOO* which adsorbed in the heterojunction surface increases the anti-bonding states compared to that of SnO₂.^[17e,25] In other words, HCOO* adsorbed in the heterojunction surface allows H* to accessibly adsorb and react with HCOO*. Maybe this is the reason why the Gibbs free energies of the RDS pathway for the formation of HCOOH declined. To obtain knowledge clearly the role of the heterojunction interface in the strong interaction between HCOO* and Sn sites, the PDOS of the catalysts model before HCOO* adsorption was analyzed. Before HCOO* adsorption, the electrons of Sn⁴⁺ tend to delocalize and donate to Cu⁺ via the O atom at the heterojunction interface (Figure S21).^[26] Consequently, the Sn atom at the heterojunction possesses high unoccupied orbitals to occupied orbitals ratio, which can promote the hybridization and bonding with the adsorbates efficiently.^[27] Therefore, all these DFT results suggest that the Sn atom in SnO₂ was activated by the formation of heterojunction interface with CuS or Cu₂O,

the activated Sn atom are easier to drag the O atom in adsorbed HCOO* and promote the combination of H* and HCOO*, thereby lowering the formation energy of HCOOH.

Besides, the electrochemical impedance spectroscopy (EIS) was studied to illustrate the catalytic kinetics and trace the HCOO* concentration around the surface of SnS₂, CuS and Cu₂SnS₃ during the CO₂RR process. As shown in Figure S22, the CO₂RR of all catalysts is dominated by the charge transfer process. Benefited from the formation of heterojunction, the Cu₂SnS₃ presents a smaller charge transfer resistance than SnS₂ and CuS (Figure S22d). Meanwhile, the charge transfer resistance of the Cu₂SnS₃ exhibits strong potential-dependent (Figure 6a), indicating that the heterojunction has a faster charge transfer rate for CO₂ to Formate.^[28] What's more, the adsorbates concentration for electrocatalytic process shows positive correlation with C_q.^[29] The C_q of Cu₂SnS₃ is larger than CuS and SnS₂ with the potential raised (Figure 6b), which means that the HCOO* are easier to adsorb in the Sn of Cu₂SnS₃.^[29–30] Thus, these results also confirm that the formation of heterojunction interface via in situ electroreduction driven self-adapt transformation promotes the charge transfer and the HCOO*



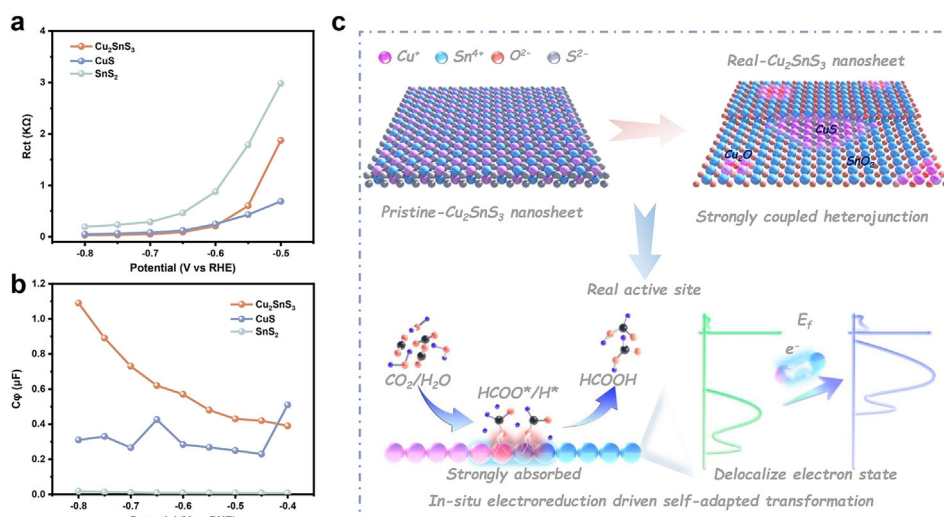


Figure 6. The catalytic mechanism. a) The R_{ct} plots for SnS_2 , CuS and Cu_2SnS_3 at different potentials. b) The C_p for SnS_2 , CuS and Cu_2SnS_3 at different potentials. c) The proposed mechanism on Cu_2SnS_3 for CO_2RR to formate.

adsorption process (Figure 6c), thereby accelerating the kinetics of CO_2 to formate.

Conclusion

Combined with structure characterization and DFT calculations, we unraveled that the active center of the ternary sulfides for CO_2RR is the CuS@SnO_2 heterojunction nanosheets with part of Cu_2O through in situ electroreduction driven self-adapt transformation. In the heterojunction interface, the electron of Sn^{4+} tend to delocalize and donate to Cu^+ via the O atom at the heterojunction interface. Consequently, the activated Sn atom in the heterojunction surface is easier to adsorb HCOO^* and raise the opportunity of the combination between H^* and HCOO^* . Benefited from the synergistic effect of stable heterojunction structure and the electron self-flow tendency, the optimized catalysts exhibit a promising combination of high activity and selectivity for CO_2 to formate over the wide potential windows from -0.6 V to -1.1 V. The present work not only reveal the true active center of the ternary sulfide, but also opened a door to design a stable and efficient electrocatalysts suitable for a wide operated potential window.

Acknowledgements

This work was financially supported by the National Natural Science Foundation of China (22071069, 21805102, and 21825103), the Hubei Provincial Natural Science Foundation of China (2019CFA002), the Foundation of Basic and Applied Basic Research of Guangdong Province (2019B1515120087). We also acknowledge technical support from Analytical and Testing Center in Huazhong University of Science and Technology.

Conflict of Interest

The authors declare no conflict of interest.

Keywords: CO_2 electroreduction · Sn catalyst · delocalized electron states · heterojunctions · phase separation

- [1] a) P. De Luna, C. Hahn, D. Higgins, S. A. Jaffer, T. F. Jaramillo, E. H. Sargent, *Science* **2019**, *364*, eaav3506; b) L. Wang, W. Chen, D. Zhang, Y. Du, R. Amal, S. Qiao, J. Wu, Z. Yin, *Chem. Soc. Rev.* **2019**, *48*, 5310–5349; c) L. Zhang, X. X. Li, Z. L. Lang, Y. Liu, J. Liu, L. Yuan, W. Y. Lu, Y. S. Xia, L. Z. Dong, D. Q. Yuan, Y. Q. Lan, *J. Am. Chem. Soc.* **2021**, *143*, 3808–3816; d) Z. W. Seh, J. Kibsgaard, C. F. Dickens, I. Chorkendorff, J. K. Nørskov, T. F. Jaramillo, *Science* **2017**, *355*, eaad4998.
- [2] a) A. Boddien, H. Junge, *Nat. Nanotechnol.* **2011**, *6*, 265–266; b) W. Wang, Q. Wen, Y. Liu, T. Zhai, *Acta Chim. Sin.* **2020**, *78*, 1185–1199; c) S. Kar, A. Goepfert, V. Galvan, R. Chowdhury, J. Olah, G. K. S. Prakash, *J. Am. Chem. Soc.* **2018**, *140*, 16873–16876; d) Q. Yang, X. Guo, Y. Liu, H. Jiang, *Int. J. Mol. Sci.* **2021**, *22*, 1890.
- [3] a) S. Nitopi, E. Bertheussen, S. B. Scott, X. Liu, A. K. Engstfeld, S. Horch, B. Seger, I. E. L. Stephens, K. Chan, C. Hahn, J. K. Nørskov, T. F. Jaramillo, I. Chorkendorff, *Chem. Rev.* **2019**, *119*, 7610–7672; b) M. G. Kibria, J. P. Edwards, C. M. Gabardo, C. T. Dinh, A. Seifitokaldani, D. Sinton, E. H. Sargent, *Adv. Mater.* **2019**, *31*, 1807166.
- [4] a) N. Han, P. Ding, L. He, Y. Li, Y. Li, *Adv. Energy Mater.* **2020**, *10*, 1902338; b) S. Zhao, S. Li, T. Guo, S. Zhang, J. Wang, Y. Wu, Y. Chen, *Nano-Micro Lett.* **2019**, *11*, 62; c) J. T. Feaster, C. Shi, E. R. Cave, T. Hatsukade, D. N. Abram, K. P. Kuhl, C. Hahn, J. K. Nørskov, T. F. Jaramillo, *ACS Catal.* **2017**, *7*, 4822–4827.
- [5] a) A. Dutta, A. Kuzume, M. Rahaman, S. Veszteg, P. Broekmann, *ACS Catal.* **2015**, *5*, 7498–7502; b) Z. Li, A. Cao, Q. Zheng, Y. Fu, T. Wang, K. T. Arul, J. L. Chen, B. Yang, N. M. Adli, L. Lei, C. L. Dong, J. Xiao, G. Wu, Y. Hou, *Adv. Mater.* **2021**, *33*, 2005113; c) J. Gu, F. Heroguel, J. Luterbacher, X. Hu, *Angew. Chem. Int. Ed.* **2018**, *57*, 2943–2947; *Angew. Chem.* **2018**, *130*, 2993–2997.
- [6] a) C. Liang, B. Kim, S. Yang, Y. Liu, C. F. Woellner, Z. Li, R. Vajtai, W. Yang, J. Wu, P. J. A. Kenis, P. M. Ajayan, *J. Mater. Chem. A* **2018**, *6*, 10313–10319; b) K. Wang, D. Liu, P. Deng, L. Liu, S. Lu, Z. Sun, Y. Ma, Y. Wang, M. Li, B. Y. Xia, C. Xiao, S. Ding, *Nano Energy* **2019**, *64*, 103954; c) W. Xie, H. Li, G. Cui, J. Li, Y. Song, S. Li, X. Zhang, J. Y. Lee, M. Shao, M. Wei, *Angew. Chem. Int. Ed.* **2021**, *60*, 7382–7388; *Angew. Chem.* **2021**, *133*, 7458–7464.
- [7] a) W. Ju, F. Jiang, H. Ma, Z. Pan, Y. B. Zhao, F. Pagani, D. Rentsch, J. Wang, C. Battaglia, *Adv. Energy Mater.* **2019**, *9*, 1901514; b) Q. Li, J. Fu, W. Zhu, Z. Chen, B. Shen, L. Wu, Z. Xi, T. Wang, G. Lu, J. J. Zhu, S. Sun, *J. Am. Chem. Soc.* **2017**, *139*, 4290–4293; c) P. Wang, M. Qiao, Q. Shao, Y. Pi, X. Zhu, Y. Li, X. Huang, *Nat. Commun.* **2018**, *9*, 4933.

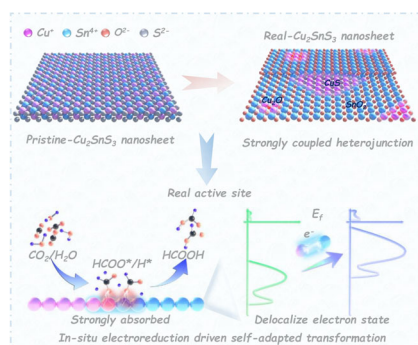
Research Articles



Electrochemistry

W. B. Wang, Z. T. Wang, R. O. Yang,
J. Y. Duan, Y. W. Liu,* A. M. Nie, H. Q. Li,
B. Y. Xia, T. Y. Zhai* ——— ■■■■—■■■■

In Situ Phase Separation into Coupled
Interfaces for Promoting CO₂
Electroreduction to Formate over a Wide
Potential Window



Cu₂SnS₃ evolved into the strongly coupled heterogeneous interfaces of SnO₂@CuS and SnO₂@Cu₂O under reaction conditions. This strongly coupled heterojunction as real active sites driven the electron self-flow from Sn⁴⁺ to Cu⁺, thus promoting the delocalized Sn sites to combine HCOO* with H*. Thus, Cu₂SnS₃ nanosheets achieve over 83.4% formate selectivity in a wide potential range from -0.6 V to -1.1 V.

